Effect of Microstructure and Temperature on Nuclear Graphite Oxidation Using the 3D Random Pore Model[1]

Ryan M. Paul[2], Jose D. Arregui-Mena, Cristian I. Contescu, Nidia C. Gallego

Oak Ridge National Laboratory, Oak Ridge, TN 37830

Abstract

This work compared the 3D Random Pore Model (3D-RPM) with experimental and characterization data to systematically study the effect of nuclear graphite microstructure and air oxidation temperature. It is well known that oxidation-induced weight loss at elevated temperatures degrades graphite structure and properties; however, a fundamental understanding of the role of graphite microstructure is still unclear. In this work, three diverse grades of nuclear graphite—IG-110, NBG-18, and PCEA—were examined and tested at air oxidation temperatures of 600, 650, 700, and 750°C following ASTM D7542. The 3D-RPM reproduced the microstructure and temperature dependence of mass loss curves for these grades. For the first time, measurements and modeling were combined to show how bulk density and the amount and spatial distribution of open and closed porosity affects oxidation. IG-110 was less dense and had an open pore network that is finer and more uniformly spread, and showed fastest oxidation. PCEA porosity was less uniform and showed less oxidation, while NBG-18 was more dense, had the least fine and uniform porosity, and showed the slowest oxidation. In general, oxidation proceeds faster if open porosity is more uniformly distributed and can incrementally access closed pore surface area with more ease.

[2] Corresponding author. Tel: 865-341-0674. E-mail: paulrm@ornl.gov (Ryan M. Paul)

Keywords: nuclear graphite, oxidation, porosity, microstructure, reactivity

Highlights:

- A 3D microstructural model reproduced the oxidation mass loss trends of three diverse grades at four different oxidation temperatures.
- In the microstructure, the amount of open and closed pores and their proximity to each other are important factors.
- The intrinsic reactivity of high-purity graphite is approximately independent of grade and follows expected temperature scaling for oxidation in air.
- Even in kinetic regime oxidation, there can be a density gradient in a sample due to the spatial distribution of porosity and sample size effects.

1. Introduction

Manufactured graphite materials have been critical to the advancement of energy generation and energy storage for over 100 years. In particular, high-purity graphite has been used in nuclear energy because of its low neutron absorption and high scattering cross section [1, 2]. Various designs of gas-cooled reactors have employed graphite as a neutron moderator and reflector material, including the Magnox and Advanced Graphite Reactor designs in the United Kingdom and Generation IV high-temperature reactors in the United States and other countries [1–3].

Manufactured graphite is a composite, with filler, binder, and void (porosity) phases in the microstructure. The porosity is typically 15–25% of the volume, dependent on the raw materials and processing methods [1], which poses a unique challenge when used in design as an engineering material. Graphite exhibits quasi-brittle behavior, in that is has a relatively low strain to failure and exhibits variability in its strength but does have limited damage tolerance [4-6]. Given the variability in strength, stochastic methods, such as Weibull failure probability statistics, are recommended for assessing the integrity of nuclear graphite components [4–6].

Complicating matters is that, during reactor operation, graphite is exposed to neutron irradiation, which changes its properties [7]. In this respect, the porosity in graphite helps accommodate the irradiation-induced expansion of the graphite lattice. However, simultaneously to irradiation there is potential graphite degradation due to reactions with oxidizing gases that result in mass loss. Graphite, a form of carbon, reacts with gases, such as O_2 and H_2O, to form CO and CO_2, and nuclear graphite components could be exposed to oxidizing gases in short or long duration time scales. Oxidizing gases could reach hot graphite components in the rare case of an ingress incident for hours or days, or trace amounts of oxidizing gases contained in inert coolant gases could flow over graphite surfaces for years [8–10].

Because graphite is porous, oxidation mass loss can occur at pore walls inside the material and at the external surface. Although the internal oxidation mass loss decreases apparent density, the main concern is the decrease in mechanical strength, decrease in elastic modulus, and increase in thermal conductivity that accompanies the increase in porosity [11, 12]. These effects, among others, must be considered in reactor design [5].

One challenge in predicting oxidation and its effects is the diversity of nuclear graphite grades that graphite manufacturers have developed. Since the beginning of the nuclear age in the 1940s, dozens of different grades have tested for nuclear reactors, with a select few reaching production status. No two grades are exactly alike [13, 14]. Modern nuclear graphite grades are expected to meet purity and thermal expansion isotropy targets [15], but properties depend on the raw materials, particle sizes, forming methods, and other processing steps used. Within one grade, intra-billet variation and billet-to-billet variation must also be considered [16, 17]. There could also be changes over time to raw material supply.

It is well known that oxidation behavior may be very different depending on the grade. Measured isothermal oxidation rates between different grades have been observed to vary by up to a factor of four when oxidized at 600°C [18–20]. The spread observed between grades might decrease with an increasing oxidation temperature [21]. Furthermore, within a grade, measured rates also show scatter from sample to sample [18–20].

Both microstructural and environmental factors make it challenging to predict graphite mass loss, specifically the decrease in density as a function of depth from the surface and its dependence on the graphite grade, dimensions, oxidation temperature, and type of oxidizing gas [22–24]. There are many published works on nuclear graphite oxidation, some of which have sought to address the effect of microstructure between different grades by using advanced techniques [18–36]. Recently, an increased understanding of the fundamentals of high-purity graphite oxidation emerged by using well-designed experiments and novel modeling and simulation approaches [18–36]. However, important questions remain regarding the individual role and interaction of the microstructure, size, and oxidizing environment. The exact role of graphite microstructure is not sufficiently clear, and the current state-of-the-art cannot explain the differences observed in oxidation behavior between grades. Also, no validated model is available to directly answer the question density decrease as a function of depth for a given graphite and oxidizing environment based on microstructural and environmental inputs.

This paper presents a systematic look at the microstructure and temperature dependence of graphite air oxidation in the kinetic regime based on the 3D Random Pore Model (3D-RPM) created by Paul et al. [34–36]. The 3D-RPM directly incorporates the effect of graphite microstructure on observed oxidation mass loss and makes testable predictions for the effect of sample size and

oxidation temperature. The 3D-RPM separates the effect of intrinsic reactivity, pore structure evolution, bulk density, and sample size and shows how these factors affect the overall observed mass loss [34–36]. Although previous work by the authors [34–36] compared the 3D-RPM with available published experimental data and found acceptable agreement for degree of overall mass loss, the model had not yet been tested against a well-controlled experimental matrix performed in one laboratory in which detailed information on each run were available and sample size was held constant.

In this paper, the background covers a summary of RPMs and the contributions made with the 3D-RPM [34–36] over past models. Next, the graphite samples and ASTM D7542 [37] oxidation procedure are presented. Experimental data were collected for grades IG-110, PCEA, and NBG-18 for air oxidation temperatures of 600, 650, 700, 750°C within the kinetic regime. By selecting these grades and temperatures, a wide range of observed oxidation rates were included in the study. Additionally, the methods used to obtain detailed 3D reconstructions of graphite pore structure by using X-ray computed tomography are described. Following, the results are presented, first with a direct comparison of 3D-RPM results to experimental data, and second with a close look at the pore structure differences between the graphite grades that lead to oxidation differences. The role of the open pore network in graphite is particularly scrutinized. It is discussed and concluded that the combination of pore structure modeling and advanced characterization presented here has provided a further understanding of how pore structure differences between grades contribute strongly to their oxidation behavior. This is an important step in the ongoing work to construct a predictive understanding of graphite oxidation that is based on microstructure and not on descriptors such as grain size category or forming method. Ultimately, work is building towards the microstructure-property relationships needed to assist designers and operators in assessing the impact of oxidation on graphite integrity for larger scale components used in high-temperature nuclear reactor designs. Modeling tools will be helpful but may not replace monitoring and testing of graphite components in actively operating reactors. Oxidation, irradiation, and other graphite degradation mechanisms are important components of the USA Department of Energy's Advanced Reactor Technologies R&D Program on Graphite that has been active since 2005 [3].

2. Background

2.1. Random Pore Models

RPMs for heterogeneous gas-solid reactions in porous materials were developed in the 1980s based on the statistical principle of 'extended volume' that was previously applied to the study of phase transformations in materials science [38–47]. The significance was in making the connection between the measurable apparent reaction rate, the pore structure, and the constant intrinsic reaction rate occurring at the pore walls. For systems in which there is a maximum observed in the apparent rate, it is because the rate is proportional to the growth and eventual coalescence of porosity (the apparent rate follows the trend of surface area).

A commonly used analytical form of the RPM is written in terms of a single structure parameter that is convenient for fitting to experimental data [38, 43–45]. However, several assumptions behind this form of the RPM are not always clearly presented. Pores are assumed to be overlapping cylinders (i.e., pores grow radially with reaction). Therefore, this paper refers to RPMs based on cylindrical pores as *2D-RPMs*. Additionally, all porosity is assumed to be open porosity in an infinite medium. That is, there are no initially closed pores, and no accommodation is made for sample size and shape. At a minimum, these are generally incorrect assumptions for graphite oxidation; however, the effect of these assumptions on the meaningfulness of 2D-RPMs has not been established. Although several 2D-RPM variations have been published [46–49], the convenience of the original analytical form has made it the one that has been applied to nuclear graphite oxidation. Unfortunately, the 2D-RPM has not been applied to graphite oxidation in a consistent way, leading to a wide range of reported structure parameters without an underlying connection to the graphite microstructure or oxidation test conditions [43–45] and thus preventing a clear microstructure-based understanding of graphite oxidation.

2.2. 3D-Random Pore Model

Recently, the 3D-RPM [34–36] was developed as an alternative to 2D-RPMs and improve the ability to model nuclear graphite oxidation. In the 3D-RPM, porosity comprises randomly placed spheres, which form a network of pore clusters, as a simplified representation of the pore structure in graphite. The remainder of the structure is solid graphite. The spheres enlarge in three dimensions because of constant reactions at the sphere wall surface area. In support of spheres as an improvement over cylinders, Paul et al. [36] showed that pores in a small graphite sample grew

in 3D with oxidation and thus did not match the 2D growth assumed in 2D-RPMs. Furthermore, in the 3D-RPM there are initially closed pores in a sample that do not participate in a reaction until they are discovered by growing open pores and thus become connected to the external surface. Additionally, sample size is explicitly considered because oxidation starts at an external surface and moves inward. The 3D-RPM predicts the pore volume in the sample as a function of depth and the overall pore volume, which is converted to overall density and then mass. Oxidation is assumed to be in the kinetic regime, meaning that the oxidation rate is much slower than the gaseous diffusion rate of the oxidant and the product in the open pore structure. Gaseous diffusion itself is not directly modeled. Instead, all open pore wall surface area is assumed to be exposed to the same concentration of oxidant as the bulk gas and thus has the same intrinsic reactivity rate [34–36].

To illustrate the 3D-RPM, Figure 1 provides a longitudinal cross section of a cylindrical graphite sample with symmetry at the centerline, containing randomly placed spherical pores. Randomly placed spherical pores are not drawn to scale and are intentionally exaggerated in size for the sake of the illustration. During an oxidation test, the cylinder is exposed to flowing hot air, and the oxidant can access the internal open pore structure of the graphite from the radial external surface. Oxidation from the top and bottom of the cylinder is neglected. At $t = 0$, there are pores that are initially connected to the external surface (i.e., open pores) and pores that are not (i.e., closed pores). Oxidation reactions only occur inside the open pores at the pore walls. The open pore region initially extends a certain depth below the external surface (radius of r^{op}). However, as oxidation reactions remove carbon from the walls of open pores, they grow in size and connect to (i.e., discover) pores that were previously closed. The rate of discovery is assumed to occur at a constant rate inward. The discovered and newly open pores that are at some depth below the surface can now grow, and they grow at the same rate as original open pores. However, because it took time for discovered pores to open, their growth is not as large at a given time as pores closer to the external surface (see $t = t_1$ and $t = t_2$). Eventually, there are no closed pores [34–36]. As oxidation progresses over time, this leads to a density profile in the sample that is a function of microstructure and oxidation temperature. Because of the kinetic regime assumption, the overall reaction is not limited by gaseous diffusion, but by the growth rate of open pores and the pore discovery rate.

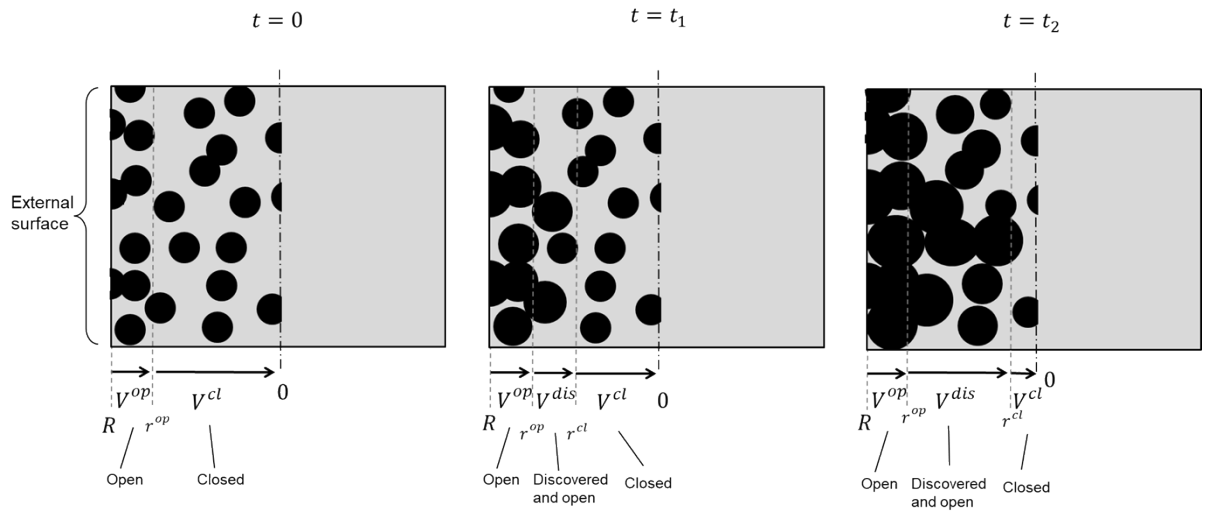

Figure 1*. Cross section of a cylindrical graphite sample with symmetry at the centerline showing randomly placed spherical pores and different regions of porosity. Pore sizes are exaggerated for effect. Oxidation moves inward from the external surface from t = 0 [34–36].*

Mathematically, the sample volume is divided into three regions that are treated independently, as shown in Figure 1. The concept of extended volume is used to account for the overlap between spheres that are randomly placed and grow isotropically. The complete 3D-RPM derivation was previously published in full [34–36]; the following is a summary of the equations and implications.

The total pore volume fraction (V_V) is divided into initially open pores (V^{op}), discovered pores (V^{dis}) at $t > 0$, and closed pores (V^{cl}), as defined by:

$$V_V = \frac{V^{op} + V^{dis} + V^{cl}}{V^{Total}} \tag{1}$$

where the total cylindrical volume (cylinder external radius R and height H) is:

$$V^{Total} = \pi R^2 H \tag{2}$$

The initially open pore region is defined between the cylinder radii of R and r^{op}:

$$V^{op} = \left\{1 - exp\left[-V_V^{ex,o}(1+\alpha)^3\right]\right\} \pi H (R^2 - r^{op^2}) \tag{3}$$

whereas the discovered pore region is between cylinder radii of r^{op} and r^{cl}, which grows as:

$$V^{dis} = \int_{r^{cl}}^{r^{op}} \left\{1 - exp\left[- V_V^{ex,o}[(1+\alpha) - \beta(r^{op} - r)]^3\right]\right\} 2\pi H r dr \quad (4)$$

The initially closed pore region shrinks with time following the cylinder radius r^{cl} as the aforementioned discovered pore region grows:

$$V^{cl} = \left\{1 - exp\left[- \left(V_V^{ex,o}\right)^3\right]\right\} \pi H r^{cl^2} \quad (5)$$

For model inputs, first the external cylindrical dimensions would be readily measurable. Second, the sample bulk density would also be readily measurable and used to determine the extended pore volume with the assumption that fully dense graphite is 2.26 g/cm^3:

$$V_V^{ex,o} = -\ln\left(\frac{bulk\ density}{2.26}\right) \quad (6)$$

Third is the dimensionless oxidation time, α:

$$\alpha = \frac{k}{r_o} t \quad (7)$$

in which k/r_o is the intrinsic reactivity rate (units: 1/s), where k is the reaction rate (units: m/s) and $r_o$is the pore sphere radius (units: m), and time t is the real time since oxidation initiated (units: s).

Fourth is the pore discovery rate, β, in units of m^2/m^3:

$$\beta = \frac{k}{r_o K} \quad (8)$$

where K is the rate at which the discovered pore boundary moves radially inward (units: m/s) [34-36]. Accordingly, cylinder radius $r^{cl} = r^{op} - Kt$.

The 3D-RPM is solved at each dimensionless time step (step size 0.025) using MATLAB. From Eq. (1), the overall sample bulk density can be calculated as a function of dimensionless time, and afterward, overall sample mass can be calculated by using the sample dimensions. To convert from dimensionless time to real time, dimensionless time is divided by the intrinsic reactivity via Eq. (7) for a given oxidation temperature.

The main model factors are: original bulk density, sample radius and height, intrinsic reactivity, and pore discovery rate. To illustrate these effects, plots of mass fraction remaining vs. dimensionless time are shown in Figure 2, in which original bulk density, sample diameter, and

discovery rate are varied. In the top left plot, bulk density was varied from 1.6 to 1.9 g/cm^3 and in the top right plot cylinder diameter was varied from 0.25 to 5 cm. In the bottom plot, pore discovery rate was varied from 5 to 1000 m^2/m^3. The effect of intrinsic reactivity itself is built in because plotting the factors against dimensionless time condenses all reactivity values onto one plot. Increasing the initial bulk density slows mass loss, as does increasing the cylindrical sample diameter or decreasing the pore discovery rate.

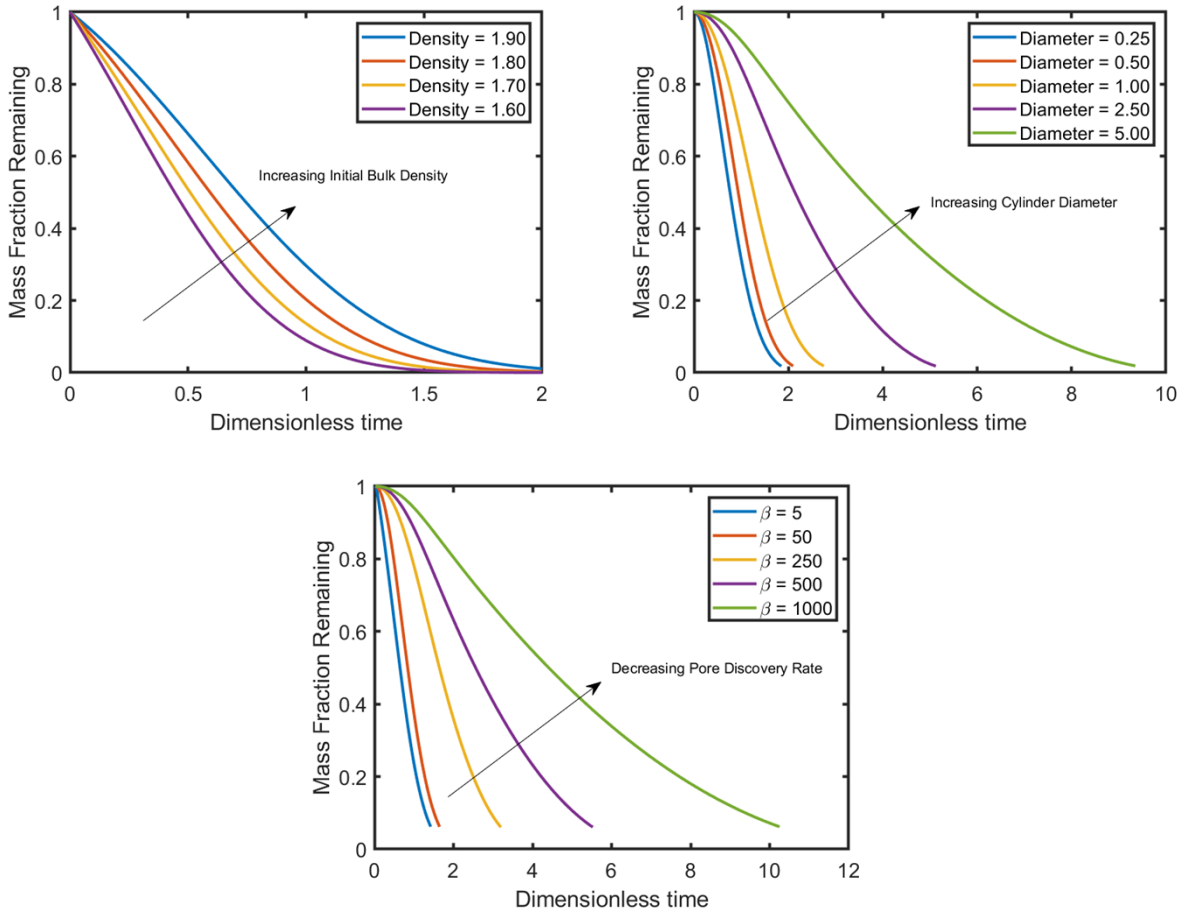

Figure 2. *Model factors in the 3D-RPM [34–36]. Plots of mass fraction remaining vs. dimensionless time illustrate the individual effects of bulk density in units of g/cm^3 (top left), cylinder diameter in units of cm (top right), and pore discovery rate in units of m^2/m^3 (bottom).*

2.3. Updated 3D-RPM Parameters

Previously published work compared the 3D-RPM to 30 air oxidation datasets that included seven different grades of nuclear graphite reported in the literature by different researchers [34–36]. The work included air oxidation temperatures from 450 to 750°C, covering essentially the entire range of temperatures that are practical for measuring air oxidation in the kinetic regime. Furthermore,

various sample sizes were included in the datasets. The deviation of weight loss values between the model and experimental data was generally within 5% [36].

Since the previous publications, the state of the model has improved by analyzing new data. The most recent results show that the intrinsic reactivity for air oxidation for high-purity nuclear grades is approximated by Arrhenius behavior with an average activation energy of 191 kJ/mol. Independently, recent work [19] showed that 191 kJ/mol was the average activation energy of six different nuclear graphite grades and therefore is further experimentally justified. To be clear, pore size itself is not an independent input parameter in the model, as differences in pore size between grades are normalized in the input intrinsic reactivity. Individual values of intrinsic reactivity extracted from 44 datasets are shown on a semi-log Arrhenius plot in Figure 3, as indicated by the fitted line. The underlying data are provided in the Supplemental Information Table A1. The fit is improved from previous work and covers the entire practical temperature range of kinetic regime oxidation, namely 450 to 750 °C.

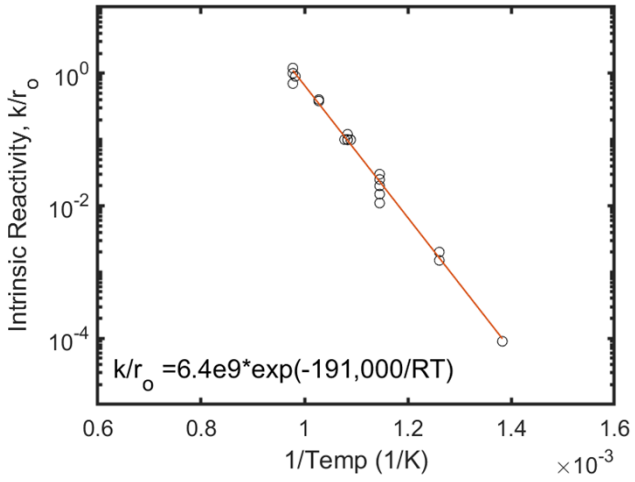

***Figure 3**. Semi-log Arrhenius plot of intrinsic reactivity, $\frac{k}{r_o}$, for 44 datasets of high-purity nuclear graphite oxidized in air taken from published data and fit with the 3D-RPM. The best fit line and equation approximates the temperature dependence fit used for the 3D-RPM.*

In addition to an improved fit for intrinsic reactivity, the understanding of pore discovery rate ratio has progressed. The units of β are m^2/m^3 and represent the incremental surface area enlargement (normalized to unit bulk graphite volume) required for the open pore network to discover closed

pores during oxidation. Because there were no direct experimental measurements available, β values were set based on fitting to experimental data for mass loss for the graphite grades. The fitting for each dataset took into account the oxidation temperature, bulk density, and sample size [34-35]. Given the degree of scatter that is observed in oxidation testing, values of β were fit as an upper and lower range, reflecting the heterogeneity in graphite structure and potential sample-to-sample and positional variations.

It has been found that there was a consistent difference in β values between graphite grades, and grain size category appeared to be a large factor. Since then, model parameters published in [34] were critically reviewed and used to test the model against the experimental data recently published in [19]. As a result of comparing the model to the new data, β ranges were slightly revised to ensure consistency. The current result is that β has now been tested against 44 datasets covering seven different nuclear graphite grades and sample sizes spanning several orders of magnitude. This evaluation has confirmed a strong effect of grain size category but also revealed an interesting finding. Specifically, as listed in Supplemental Information Table A1, ranges for finer grain grades IG-110, IG-430, and NBG-25 were on the lower end of β and coarser grain grades NBG-17 and NBG-18 were on the higher end. That is, finer grain grades trended around ranges of 300 to 600, while coarser grain grades trended around 1500 to 2200. PCEA is a coarser grade similar to NBG-18 but its β ranges of 500 to 600 were closer to the finer grain grades, and this finding was further explored in the present study as to why this was the case.

3. Materials and Methods

3.1. Graphite Grades and Samples

In this work, oxidation testing was performed on three different grades of nuclear-grade graphite. The three grades were selected because they represent a wide range of different microstructures due to differences in grain sizes and forming methods. As shown in Table 1, the three grades were IG-110, NBG-18, and PCEA and were obtained directly from the manufacturer. IG-110 is an isostatically molded superfine grain grade. NBG-18 and PCEA are both medium grain grades, but they have different grain size distributions; also, NBG-18 was vibrationally molded, whereas PCEA was extruded.

***Table 1**. Nuclear graphite grades studied in this work.*

Grade name	Manufacturer	Grain size and category	Forming method	Bulk density (g/cm^3)
IG-110	Toyo Tanso	Superfine grain, <40 μm	Isostatically molded	1.80 (n = 6)
NBG-18	SGL Carbon	Medium grain, <1.6 mm	Vibrationally molded	1.86 (n = 6)
PCEA	GrafTech (now Amsted Graphite Materials)	Medium grain, <0.8 mm	Extruded	1.79 (n = 6)

Grade samples were machined to cylinders with a nominal diameter of 25.4 mm and height of 25.4 mm. The bulk density listed in Table 1 for each grade is the average of the six machined cylindrical samples.

Differences between the grades are very apparent visually. Figure 4 is a collection of optical micrographs taken with cross-polarized light on polished sections of IG-110, PCEA, and NBG-18. In IG-110, the pore structure comprises fine pores that are generally uniform in cross section and distributed evenly. In PCEA and NBG-18, the pore structure contains a broader distribution of cross sections that are distributed less evenly.

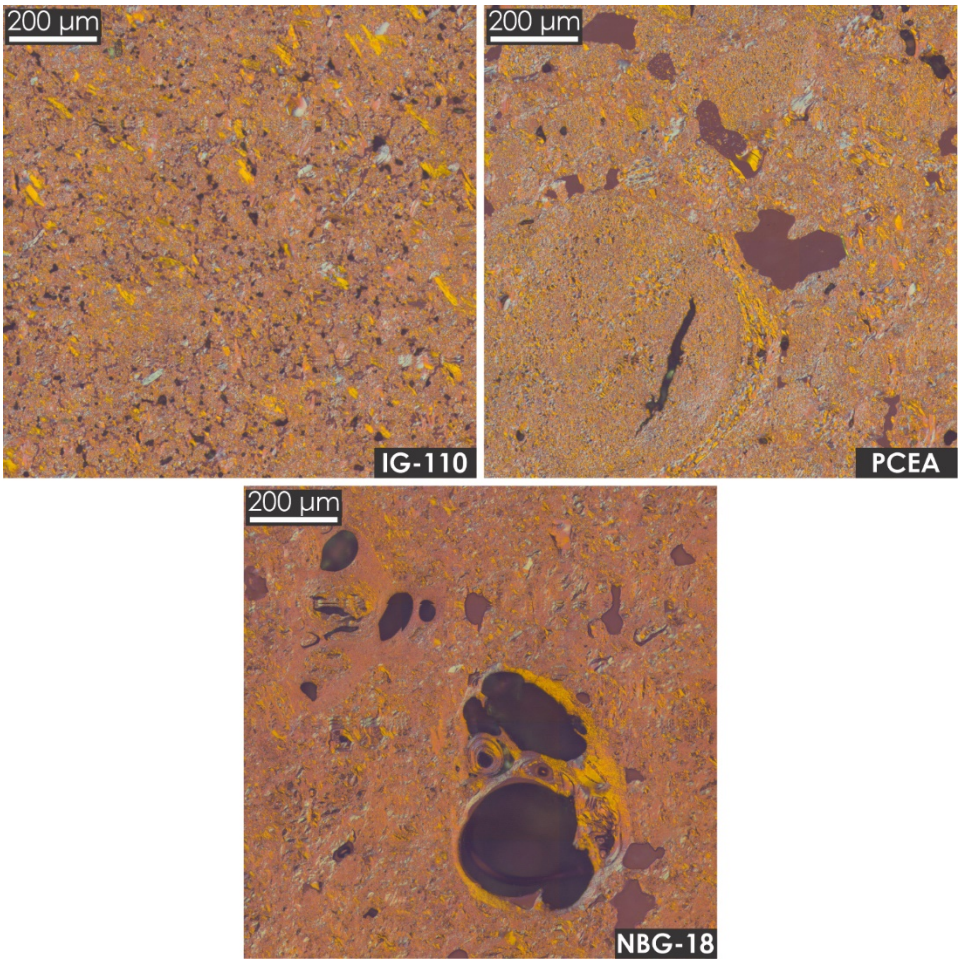

Figure 4. *Optical micrographs of nuclear graphite with cross-polarized light. The dark areas are porosity. The top left is IG-110, the top right is PCEA, and the bottom is NBG-18. The scale bar is 200 µm.*

3.2. Graphite Oxidation Procedure

Samples from the three grades of nuclear-grade graphite were tested for oxidation at four oxidation temperatures following the guidelines in ASTM D7542 [37]. Specimen and test conditions are provided in the Supplemental Information. ASTM D7542 is designed to oxidize samples in the kinetic regime. In this case, the specimen size is cylindrical with a nominal diameter and height of 25.4 mm. The specimen is suspended in a vertical tube furnace with a constant flow of inert gas while the furnace is heated to the test temperature. The gas is then switched to a constant flow of dry air at a rate of 10 L/m. The test measures the change in mass vs. the sample time due to isothermal oxidation until the mass loss reaches 15%. The standardized oxidation rate is the quasi-linear portion of the mass loss curve between 5 and 10% mass loss (i.e., 90 and 95% relative mass).

The method recommends testing a minimum of two samples at four different temperatures up to 750°C to calculate kinetic parameters for a grade of graphite following an Arrhenius approach. The kinetic parameters of interest include the activation energy (E_a, kJ/mol) and the pre-exponential factor.

3.3. X-Ray Computed Tomography Procedure

X-ray computed tomography (XCT) is a nondestructive characterization technique that was used to study the porosity of the selected graphite grades. A Zeiss Xradia 620 Versa was used to scan the samples. The instrument was operated at an acceleration voltage of 60 kV, a power of 5 W, and a current of ~83 μA. The XCT scans were cropped, segmented, and analyzed with Avizo software package version 2020.3. The segmentation process started by cropping the datasets into smaller cube subsections that were 1,150 μm on each side. Following the cropping step, the XCT datasets were segmented with a global thresholding segmentation tool incorporated in Avizo. This step used the grayscale values of the scan to classify the graphite and porosity phases. Then, the initial segmentation was further improved by using the watershed algorithm included in Avizo. XCT segmented data were processed for three purposes: to estimate and illustrate the differences between open and closed porosity across the selected graphite grades, to create pore network models (PNMs) of the open porosity, and to mimic the uniform oxidation of graphite by using the gradual dilation of the open porosity.

Open and Closed Porosity Analysis

The segmented pore content was classified as either open or closed porosity. All the pores connected directly to the exterior were classified as open porosity, and the remainder of the pores were classified as closed porosity. Longitudinal profiles across the cubes were obtained to show the distribution of open and closed porosity as a function of distance. Depth profiles of porosity were used to illustrate the spatial distribution of open and closed porosity.

Pore Network Models of Open Porosity

The open porosity labels of the selected grades were used to create their respective PNMs with the XPoreNetworkModeling Avizo extension. PNMs are representations of a pore network that use simplified geometries to depict the nodal pores as spheres and pore throats as cylinders. To

generate the PNMs, the open porosity label must be divided into smaller fractions so that these structures can be classified as either nodal or throat pores. The pores were fractioned by using two separation methods. The chamfer method was used for NBG-18 and PCEA, and the skeleton method was used for IG-110. Both separation methods apply a watershed-based algorithm to divide a label (porosity content). The chamfer method is "conservative" approach more suitable for objects or particles that tend to be round and not highly interconnected, therefore this approach was found to be more adequate for coarser grades such as NBG-18 and PCEA. In contrast the skeleton separation method is an "aggressive" approach to divide highly interconnected 3D objects formed by complex shapes such as the pore network contained in IG-110.

Open Porosity Dilation

To mimic the effects of uniform oxidation, the open porosity label was dilated with the Avizo dilation module. Dilation operations are common morphological operations for image processing and image analysis. In this case Avizo's dilation module provides multiple options to control the growth, shape, dimensions, and rules used for the generation of new voxels during each dilation step. For this research the ball dilation option was used to simulate a gradual isotropic growth of the pores by only growing 1 voxel at a time. The dilation process was repeated five times to observe the gradual growth of open porosity in IG-110 and NBG-18 due to uniform oxidation and to show the rate at which close porosity becomes open porosity as a function of the dilation step.

4. Results

4.1. Modeling of Oxidation Data

Figure 5 shows individual plots of mass vs. time for the three grades of nuclear graphite for four different oxidation temperatures, resulting in 12 plots. Marker symbols are experimental data, and two sets of data are shown for each condition. Mass loss occurs smoothly and continuously from the original mass up to where the test stops at approximately 15% mass loss. Mass loss rate is highly dependent on oxidation temperature, as indicated by the different time scales. Oxidation could reach 15% in 30–100 h at 600°C or in 1–3 h at 750°C. Furthermore, there are large differences between the graphite grades. At 600°C, there is nearly a factor of 3 difference in oxidation rates between IG-110 and NBG-18.

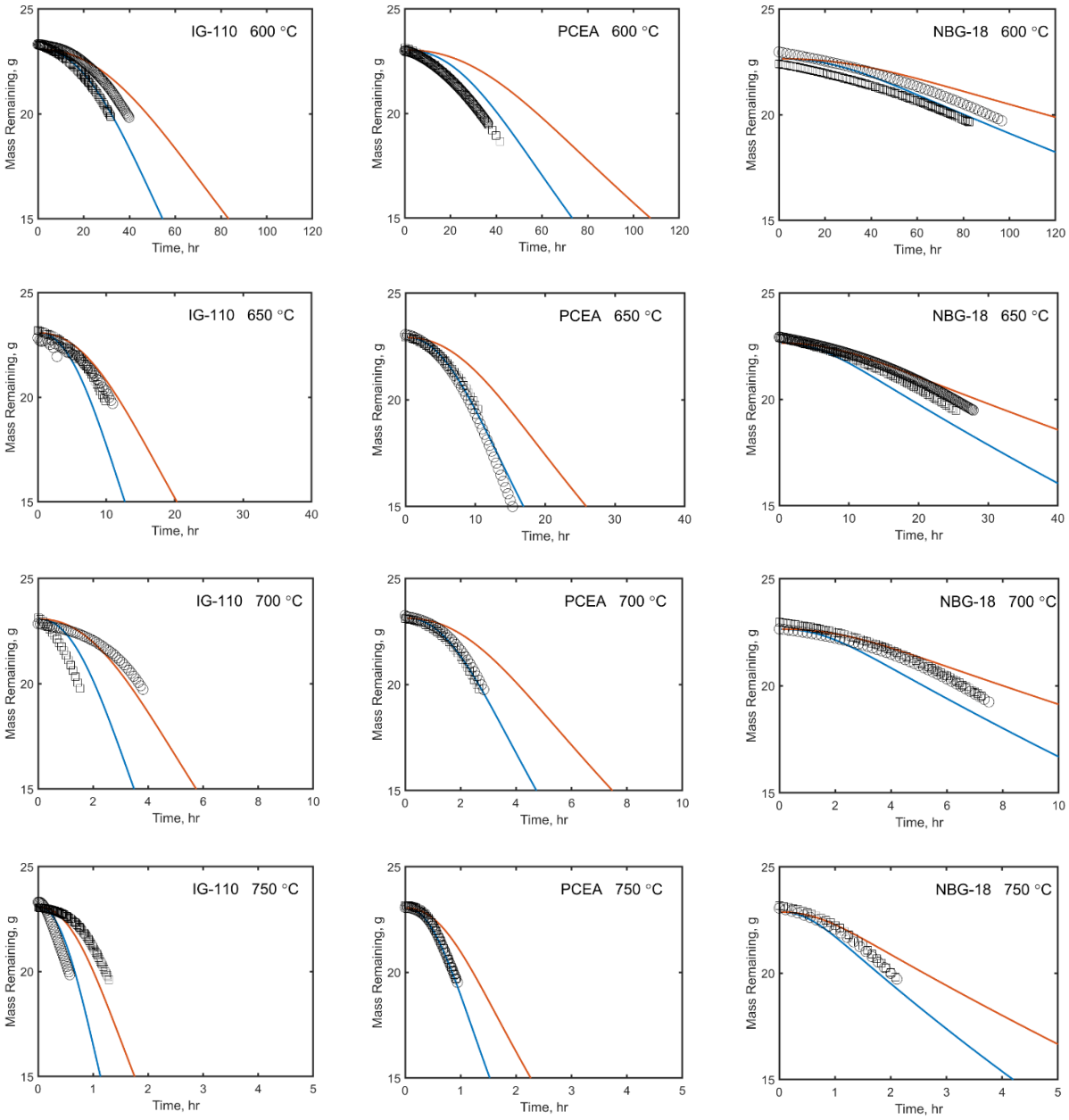

***Figure 5**. Mass vs. time during isothermal oxidation for IG-110, PCEA, and NBG-18. Open marker symbols are experimental data. Red and blue lines are model results. Model results generally bound the experimental data or capture the trend.*

The solid lines in Figure 5 are the 3D-RPM results based on model parameters k/r_o and β and the bulk density for each sample. The parameters used to generate the predictions are shown in Table 2. The upper and lower intrinsic reactivity k/r_o parameters shown in the table are +/-15% from the baseline equation from Figure 3. The red solid lines are the lower intrinsic reactivity value

combined with the higher β value, and the blue lines are the opposite combination. As previously discussed, intrinsic reactivity values were independent of grade and only a function of oxidation temperature. For the pore discovery rate ratio, β, there are systematic differences between the grades. β values were 300–400 for IG-110, 500–600 for PCEA, and 1,800–2,100 for NBG-18. A smaller value of β means that the pore discovery is occurring faster; therefore, IG-110 has the fastest pore discovery and NBG-18 has the slowest.

***Table 2**. Summary of parameters used in 3D-RPM to compare with experimental data.*

Grade name	**k/r_o, 600°C (1/s)**	**k/r_o, 650°C (1/s)**	**k/r_o, 700°C (1/s)**	**k/r_o, 750°C (1/s)**	**β (m^2/m^3)**
IG-110	0.020, 0.026	0.082, 0.111	0.296, 0.400	0.950, 1.250	300, 400
PCEA	0.020, 0.026	0.082, 0.111	0.296, 0.400	0.950, 1.250	500, 600
NBG-18	0.020, 0.026	0.082, 0.111	0.296, 0.400	0.950, 1.250	1,900, 2,200

As shown in Figure 5, the trends in experimental data for different graphite grades and oxidation temperatures are generally bounded by the model predictions. Scatter in oxidation testing among samples from the same grade is routinely observed, which is one reason why predictions are given as a range. Although the experimental data were collected up to 15% mass loss in most cases, the model results are shown at higher mass loss levels to show how the spread in the predicted range increases with time.

4.2. Pore Structure Characterization

3D reconstructions of PNMs from XCT for the three grades are shown in Figure 6 in which individual pores appear as their equivalent spherical diameter following the color code in the figure legend. Blue pores are finer while red pores are coarser. The network models highlight the differences in microstructure between the grades. For IG-110, the pore structure contains a highly connected network of fine pores and channels that are spread throughout the sample volume. For PCEA, the pore structure contains a larger size distribution with less uniform spread throughout the volume. For NBG-18, the pore size distribution is even larger and is less evenly spread in the volume than PCEA.

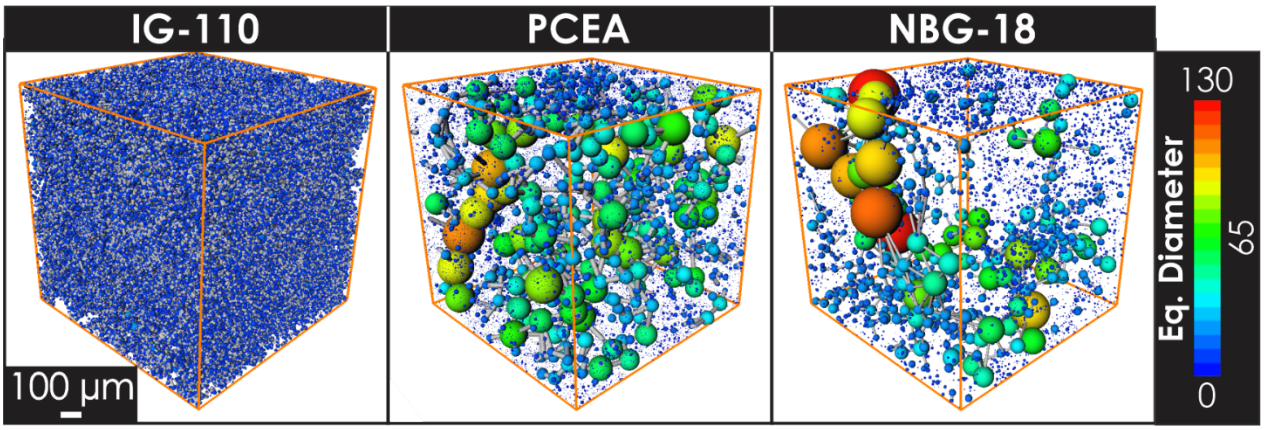

Figure 6*. 3D PNMs from XCT for the three grades. Pores are shown as their equivalent spherical diameter following the color code shown in the legend. IG-110 has a highly connected network of fine pores, whereas PCEA and NBG-18 contain larger size distributions and less uniform connectivity.*

The reconstructed porosity was segmented into open and closed pores. Open pores are connected to the external surface and are accessible by surrounding gases. Closed pores do not have a pathway to the external surface. The percentage and surface area of open and closed pores in each sample calculated from the XCT scans is listed in Table 3. IG-110 has the most open porosity, followed by PCEA and then NBG-18. The opposite trend is seen for closed porosity. IG-110 also has the highest open pore surface area, followed by PCEA and NBG-18, which follows the trend of open pore volume.

***Table 3**. Open and closed pore volume percentages (relative to total sample volume) and pore surface area in graphite samples from XCT.*

Grade name	Open porosity (%)	Closed porosity (%)	Total porosity (%)	Open pore area (mm^2)	Closed pore area (mm^2)	Total pore area (mm^2)
IG-110	15.1	2.1	17.3	634	123	757
NBG-18	7.2	5.1	12.3	45	186	231
PCEA	9.3	4.0	13.3	83	290	373

Taking the analysis one step further, the volume fraction of open and closed pores in a slice of material was computed by position from one side of the sample to the other. Results are shown in Figure 7 for the three samples. On the right, a single slice through each material is shown, where the solid graphite is in light gray, open pores in dark gray, and closed pores in black. On the left, the plots quantify the trends in porosity distribution. Very clearly, IG-110 contains a uniform spatial distribution of both open and closed pores in the volume. IG-110 also has the highest level of open pores. In contrast, the open pore structure of PCEA and NBG-18 is variable through the volume, dominated by large pore clusters. The closed porosity in PCEA and NBG-18 is more uniformly distributed than the open porosity. NBG-18 has more closed pores, but they are the least uniformly distributed, as evidenced by the greater curvature in the fraction by position. Closed pores in PCEA are more uniformly distributed than NBG-18, but not as much as IG-110. The trends of open and closed pores observed in this analysis are highly distinct and to our knowledge not previously reported.

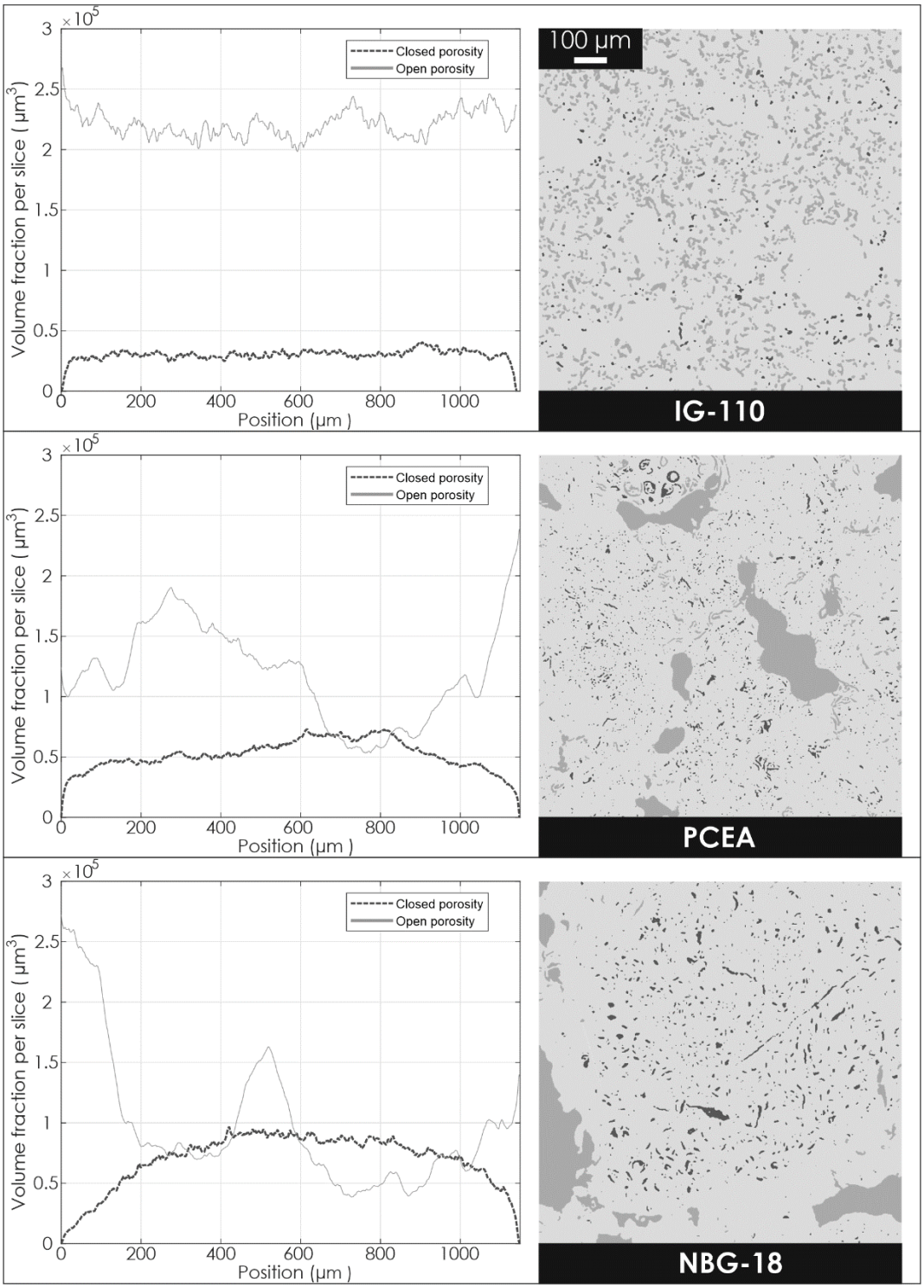

***Figure** 7. Open and closed pore volume fraction as a function of position in XCT scans. IG-110 has uniformly distributed open and closed pores, whereas PCEA and NBG-18 are dominated by large pore clusters and have less uniform distributions in the volume.*

To demonstrate the importance of the spatial distribution of open and closed pores for oxidation, an oxidation simulation was performed on the microstructure digitized by XCT. Oxidation of the open pores can be simulated with a 3D dilation of the voxel volume. In the simulation, open pores are successively dilated, which not only increased the volume of open pores incrementally but increased the volume of open pores through discovery and connection to closed pores. Results are shown in Figure 8 for IG-110 and NBG-18. As shown in the bottom plot in Figure 8 of volume fraction vs. dilation step, the simulated oxidation of IG-110 causes a significantly faster decrease in closed pores and increase in open pores than NBG-18. The relatively uniform distribution of open and closed pores in IG-110 causes easier access to closed pores as open pores incrementally grow. For NBG-18, open pores are more concentrated than IG-110, and incremental oxidation does not lead to as rapid of increase in pore volume. The accompanying microstructure cross sections shown above the plot visually reinforce the differences between the oxidation behaviors of IG-110 and NBG-18.

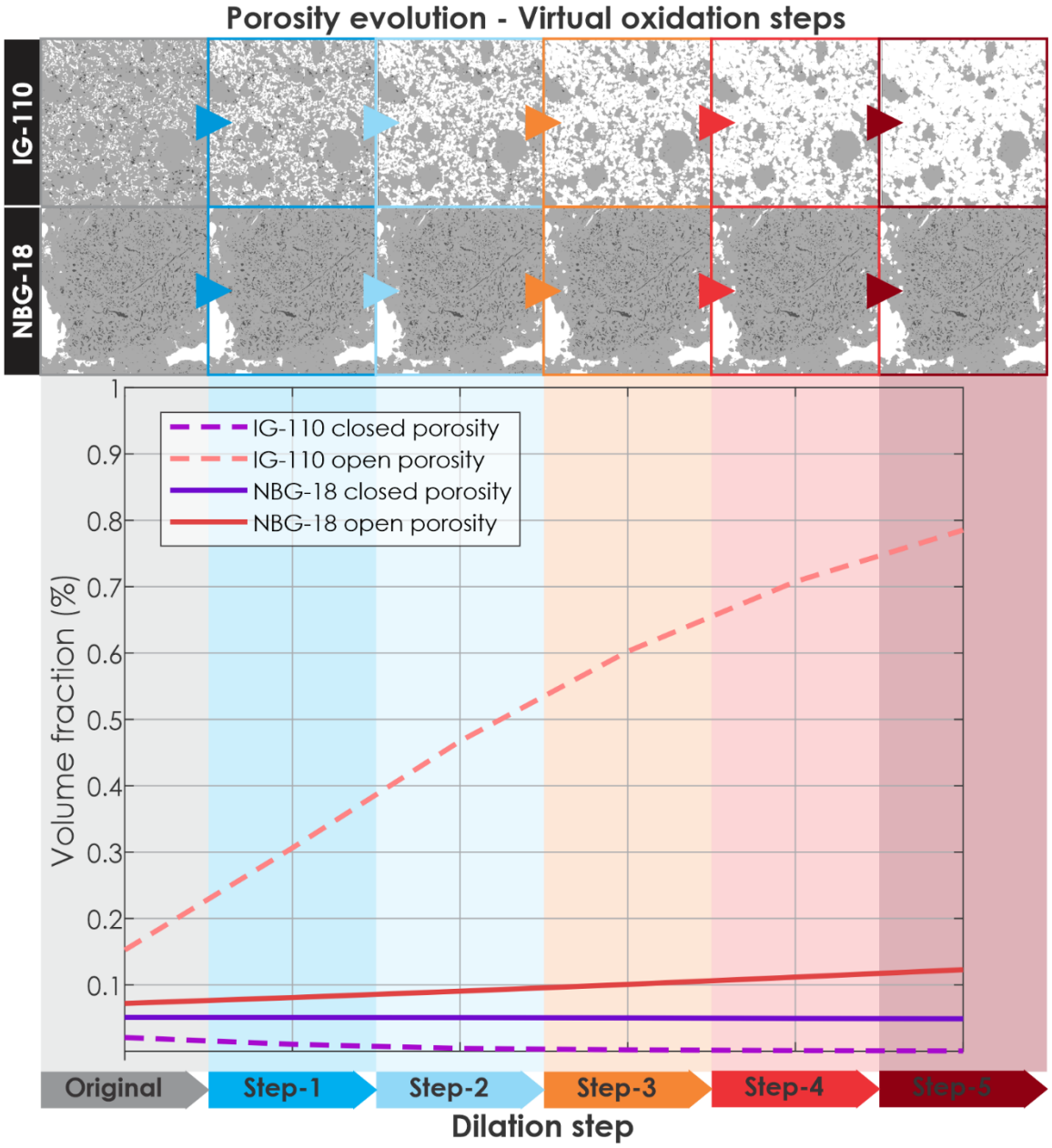

Figure 8. *Simulated oxidation using 3D dilation of pore structure from XCT. The closed pores in IG-110 are converted to open pores at a much faster rate than NBG-18, and overall oxidation proceeds faster.*

5. Discussion

This work compared the 3D-RPM with 24 sets of experimental data for three different nuclear graphite grades and four different air oxidation temperatures—all measured in one laboratory and with the sample size held constant. This work is significant because it brings together experimental data, 3D microstructural modeling, and 3D XCT characterization to put forth a mechanistic explanation for the differences in observed oxidation mass loss between grades. In contrast, previously there has not been consistency in how other RPMs have been applied to graphite oxidation, and this confusion has inhibited progress in modeling graphite oxidation. The 3D-RPM can reproduce the trends in kinetic regime mass loss that depend on microstructure and air oxidation temperature. Importantly, for the first time, XCT measurements were presented on the spatial distribution of open and closed pores and this was shown to be important for oxidation.

The 3D-RPM is a simplified mathematical representation of graphite microstructure and thermal oxidation. The pore structure of nuclear graphite is modeled as a random array of spherical pores, which create a network of open and closed pores of various cluster sizes throughout the volume. This simplification allows for solvable equations using the concept of extended volume, in the absence of a completely accurate mathematical description of graphite pores. While real pores in graphite are not perfectly spherical or clusters composed of spheres, the 3D-RPM is built on 3D growth of porosity, which is the correct growth order [36], while previous RPMs considered only 2D growth. For the 3D-RPM, porosity is located in the binder phase of graphite, as the binder phase oxidizes preferentially over the filler phase [22], at least through approximately 50% weight loss in the kinetic regime [26], which is the region of interest. Accordingly, ignoring oxidation of the larger filler particles is not considered to be a limitation for existing nuclear graphite grades where the focus is on weight loss up to approximately 30% [5]. Once oxidation begins, open pores enlarge. The rate at which pores enlarge is modeled as an intrinsic reactivity that is only temperature dependent for high-purity graphite oxidized in air. As open pores enlarge, they grow and connect to (i.e., discover) closed pores. The pore discovery rate of a graphite depends on the graphite's initial microstructure. Overall, oxidation mass loss occurs smoothly and continuously over time. Because oxidation moves inward from the external surface, oxidation is nonuniform throughout the depth, and the overall mass loss is sample size dependent. Gaseous diffusion is not directly modeled at this time because it is not considered the rate limiting step for kinetic regime

oxidation. However, future work could incorporate different oxidizing gases and diffusion-limited oxidation.

Traditionally, kinetic regime graphite oxidation (i.e., Regime I) holds that there is a constant concentration profile of oxidant—and, therefore, bulk density—inside a sample during oxidation because the oxidation reaction rate is much slower than the rate of gaseous diffusion inside the pore structure [24]. For the 3D-RPM, this view of the kinetic regime is amended so that the concentration profile is constant in the open pore structure, which continues to grow over the course of oxidation and connect to closed pores. Therefore, size effects and density gradients are compatible with kinetic regime graphite oxidation and will be influenced by the particular graphite microstructure. A sample that is oxidized in the kinetic regime could show a nonuniform bulk density profile.

Intrinsic Reactivity

In this work, the use of an intrinsic reactivity for air that is only temperature dependent for high-purity graphite is judged to be reasonable. An intrinsic reactivity that does not change with the degree of oxidation assumes that it is proportional to the reacting surface area ratio. An intrinsic reactivity that does not depend on grade assumes that there are no systematic differences at the level of the graphite reacting surface (e.g., pore size differences are normalized and that there are no catalytical impurities or degree of graphitization differences that are known to affect the intrinsic rate [50]). At this time, it is unknown how much intrinsic reactivity could vary within a sample, within a grade, or from grade to grade. Several studies have not found a clear relationship between the degree of crystallinity as measured by bulk x-ray diffraction or Raman spectroscopy and the overall oxidation rate for nuclear grades [18, 20, 51].

Gallego et al. [52] used high-resolution nitrogen adsorption, and the data showed that the ratios of active surface area (ASA) to total surface area (TSA) for IG-110, PCEA, and NBG-18 were all within 15% of their average value. The ASA was taken as the TSA minus the Langmuir surface area [52]. This technique was extended to include measurements taken on air-oxidized samples of IG-110, and the results are shown in Table 4. TSA increases significantly with oxidation, as does ASA. The ratio of ASA to TSA is reasonably similar among conditions, although there is scatter that could be due to the inherent heterogeneity in graphite. These results support the concept that

intrinsic reactivity is approximately similar for these nuclear grades and does not change with degree of oxidation.

Table 4. High-resolution nitrogen adsorption measurements [52] of TSA and ASA on unoxidized and oxidized IG-110.

Sample description	TSA (m^2/g)	ASA (m^2/g)	ASA/TSA
Unoxidized IG-110	1.18	0.95	0.81
Oxidized to 11.3% at 600°C	6.53	2.90	0.44
Oxidized to 17.8% at 600°C	11.43	7.01	0.61
Oxidized to 6.1% at 700°C	6.09	4.67	0.77
Oxidized to 23.8% at 700°C	7.62	4.53	0.59

Kane et al. [28] used an intrinsic reactivity rate with a shrinking platelet model to systematically study the oxidation of NBG-18 fine powder to eliminate pore effects and found that it was reasonably constant during most of the oxidation. In a later study, Kane et al. [26] found that the ratios of relative reactive surface area to relative TSA of IG-110 and NBG-18 were approximately constant from 10 to 55% oxidation. These independent studies also support the assumption of a constant intrinsic reactivity that is similar for high-purity graphite grades.

Pore Discovery Rate

The current work indicates that IG-110 oxidizes more quickly than NBG-18 or PCEA because its bulk density is lower and its pore network is initially more open; additionally, all pores are more uniformly distributed through the volume, bringing the open pores closer to the closed pores. As open pores enlarge, they easily connect to the nearby additional surface area of the closed pores. PCEA is coarser grained than IG-110 but is seen to have more uniformly distributed open and closed pores than NBG-18. In contrast, NBG-18 oxidizes more slowly because it is denser, its open pore network is more concentrated in fewer branches, and there are more closed pores that are less uniformly accessed. As open pores oxidize and grow in NBG-18, it takes longer for them

to connect to closed pores. Mathematically, in the 3D-RPM, the rates of pore discovery are smaller for IG-110 (β = 300–400 m^2/m^3) and larger for PCEA (β = 500–600 m^2/m^3) and NBG-18 (β = 1,900–2,100 m^2/m^3). The units of β (m^2/m^3) are a surface-to-volume ratio. The physical meaningfulness is that β is the incremental amount of surface area (per sample volume) increase needed for open pores to discover and connect to closed pores during oxidation. IG-110 has a lower β because its open and closed pores are closer in proximity. The less uniformly distributed open and closed pores in PCEA and NBG-18 correspond to higher values of β. The oxidation rates of the three grades ranked from fastest to slowest are: IG-110, PCEA, and NBG-18. On one hand this ranking order agrees with the overall open pore volume and surface area, but one must consider the spatial distribution of the pores which is why PCEA oxidizes more closely to IG-110 than NBG-18. This is the reason why PCEA, although a medium grain grade like NBG-18, shows oxidation much closer to IG-110. Therefore, one cannot rely on grain size category alone to rank oxidation behavior. While β largely remains an empirical factor in the model, additional work is underway in the form of direct experimental measurements to firmly connect it to microstructure, by analyzing the incremental evolution of porosity during oxidation.

At least for IG-110, there is a point for comparison for β. Kim et al. [55] estimated that the initial reacting surface-to-volume ratio for IG-110 was 17,260 1/m based on the oxidation of 16 samples of different sizes and shapes. In this work, the β value for IG-110 was 300–400 1/m, which is approximately 1–2% of the initial value from Kim et al. With these values, it is reasonable to assume that β could represent the incremental amount of surface area per volume needed for open pores to connect to neighboring closed ones.

The mathematical modeling of the 3D-RPM is supported by the XCT scans and simulated oxidation presented in this work. For comparison, in a thorough study, Kane et al. performed the simulated oxidation of open porosity by using the dilation of reconstructed porosity from high-resolution XCT for IG-110, PCEA, and NBG-18 [26]. The work showed that NBG-18 had larger initial closed pore volume and that as oxidation progressed, the closed pores remained closed to higher levels of oxidation, unlike PCEA or IG-110. For IG-110, the closed pores opened at lower oxidation levels, which was more similar to PCEA. For IG-110 and PCEA, closed porosity decreased to 5% of the total porosity by about 10–15% simulated oxidation, whereas to reach the same level as much as 25–35% of simulated oxidation was required for NBG-18. The findings in

Kane et al. for IG-110, PCEA, and NBG-18 mirror the trends seen in this work for the same graphite grades, even though the tomography scans in Kane et al. included larger volumes of material and had more nuanced simulated oxidation parameters than this study. Importantly, the findings in Kane et al. independently quantitatively support the ranking of pore discovery rates reported in this study for the three grades and are consistent with the mechanics and parameters of0 the 3D-RPM.

Open and Closed Porosity

While XCT is capable of providing useful insights into graphite pore structure, one must respect limitations of equipment resolution and digitization. For comparison, mercury porosimetry and gas pycnometry are well-known methods for measuring pore volume in a sample, although each has its own strengths. Data was available for the three grades in this study, from a recent report published by several of the authors [53]. Mercury porosimetry results (cumulative pore volume as a function of pore entrance diameter) for IG-110, NBG-18, and PCEA are plotted in Figure 9 [53]. The data shows that NBG-18 contained the relatively lowest overall open pore volume and contained open pores that span the entire measured range of entrance diameters. However, it did not contain as many large open pores as PCEA. The implication is that some of the large pores were closed in NBG-18 but are open in PCEA. The total open pore volume of PCEA is relatively larger, even though the size range was similar to NBG-18. IG-110 had most of its open porosity in the 2–4 micron entrance diameter range with smaller pores as the remainder. Furthermore, helium pycnometry results in the same report [53] support the ranking of open pore volume for the three grades. This is an important confirmation, due to limitations of mercury porosimetry. What is meaningful for the present study is that the porosimetry and pycnometry results reinforce the general trends from XCT: IG-110 has the largest open pore volume, followed by PCEA and then NBG-18. In addition to the trends, quantitatively the results show that PCEA has a large amount of open pore volume, nearly that of IG-110, with both having more than NBG-18. This is despite that PCEA is a medium grain grade like NBG-18. The larger amount of open pore volume contributes to the oxidation behavior of PCEA being closer to IG-110, reinforcing the importance of open porosity in the trends and mechanisms of oxidation behavior put forth in this work.

As another confirmation, the trends seen in open pore surface area from XCT shown in Table 3 are reinforced by those obtained using Kr adsorption previously published by the authors [18].

Therefore, independent testing positively supports that no systematic misinterpretation was made with the XCT results for the three graphite grades.

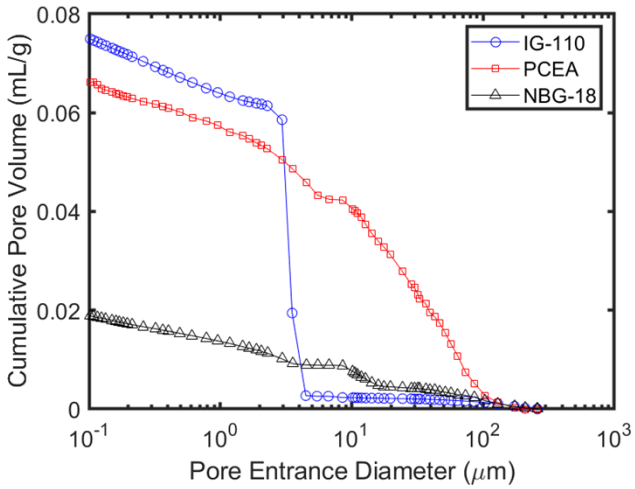

Figure 9. Mercury porosimetry cumulative pore volume as a function of pore entrance diameter for the three graphite grades. Data from the authors' recent report [53].

Future Directions

This study highlights the contributions of XCT to the study of graphite structure and properties, where its use is growing [54]. Although overall volumes and surface areas of open porosity are measurable via methods such as helium pycnometry, mercury porosimetry and gas adsorption, this study showed that the size, location, and distribution of open pores in graphite are as important as their overall amount to kinetic regime oxidation. Pore size and shape can be viewed on cross sections, but connectivity can only be examined in 3D, such as with XCT. Because XCT is limited by resolution and cannot clearly identify pores below the resolution limit, future work should combine it more systematically with porosimetry and gas adsorption techniques for comparison and validation. The digital structure of graphite from XCT is also valuable for modeling and simulation.

Although this work focused on predicting the overall mass loss versus time for different isothermal oxidation temperatures, the model is built on the concept that oxidation occurs nonuniformly through the sample depth, which leads to a density profile. Additional work is needed to study

density profiles and open and closed porosity as a function of sample size and oxidation conditions to compare with the model meaningfully and extend the usefulness.

Finally, although predicting overall and local mass loss due to oxidation is important, the greatest need is to understand the effect on mechanical and thermal properties. Properties such as strength, modulus, thermal conductivity, and thermal expansion are used to compute the integrity of graphite components, and mechanical-thermal integrity could be reduced if oxidation occurs. Future work could extend the 3D-RPM to be used in combination with structure-property models. Both reactor designers and operators will need data on the structure-property relationships for oxidized graphite grades being considered for high-temperature gas cooled reactors. Research into oxidation and other degradation mechanisms for graphite are key parts of the USA Advanced Reactor Technologies R&D Program for Graphite funded by the Department of Energy to provide data to enable the realization of an operational reactor [3].

6. Conclusions

This work combined 3D microstructural modeling and 3D characterization to demonstrate the microstructural and kinetic basis for differences in observed oxidation mass loss for nuclear graphite. 3D-RPM, the microstructural model, reproduced the air oxidation mass loss trends of three diverse grades of high-purity nuclear graphite at four different oxidation temperatures in the kinetic regime. The studied grades and temperatures span a large range of oxidation rates all measured in one laboratory by using the same oxidation setup following ASTM D7542. The model was judged to perform well compared with the available experimental data up to approximately a 15% mass loss based on parameters set by previous work.

The intrinsic reactivity of high-purity graphite is approximately independent of grade and follows expected temperature scaling for oxidation in air. Currently, there is no clear evidence that intrinsic reactivity depends on the grade or degree of oxidation. However, grades that are less pure or less graphitized must be studied separately.

Microstructure contributes significantly to the oxidation mass loss of nuclear graphite on an overall level and a local level. Initial bulk density, sample size and shape, and open and closed porosity are important factors in the model in addition to the intrinsic reactivity.

In the microstructure, the amount of open and closed pores and the proximity of the pores to each other are major factors. IG-110 has a lower bulk density and higher levels of open pores, which are more evenly distributed around closed pores. This means that the additional surface area of closed pores is more easily accessed than PCEA or NBG-18 as oxidation proceeds. Results show that grain size category alone is not an adequate predictor of oxidation, as PCEA is a medium grain grade like NBG-18, buts its oxidation behavior is closer to IG-110, a superfine grade.

Even in the kinetic regime, oxidation can lead to a density gradient in a sample. However, the true need is to connect density loss to mechanical and thermal properties for assessing the integrity of graphite components that are oxidized. The current modeling methodology can be extended to structure-property models. Future work should extend the model to include diffusion-limited oxidation and oxidizing gases other than air.

Acknowledgments

This work was supported by the US Department of Energy's Office of Nuclear Energy under the Advanced Reactor Technologies—Gas Cooled Reactor program. Oak Ridge National Laboratory is managed by UT-Battelle LLC under contract DE-AC05-00R22725.

Supplemental Information

Table A1. *Table of updated 3D-RPM parameters and fits.*

Grade name	Data reference	Oxid. temp. (°C)	k/r_o (1/s)	Upper and lower β (m^2/m^3)	Bulk density (g/cm^3)
IG-110	[20]	600	0.02	300, 400	1.77
IG-110	[58]	650	0.1	300, 400	1.67
IG-110	[56]	520	0.002	300, 400	1.79
IG-110	[56]	600	0.015	300, 400	1.78
IG-110	[57]	600	0.02	300, 400	1.76
IG-110	[57]	600	0.02	300, 400	1.76
IG-110	[57]	600	0.02	300, 400	1.76
IG-110	[27]	600	0.03	300, 400	1.79
IG-110	[27]	650	0.1	300, 400	1.79
IG-110	[59]	750	0.7	300, 400	1.77
IG-430	[20]	600	0.02	600, 800	1.82
IG-430	[56]	520	0.0015	600, 800	1.82
IG-430	[56]	600	0.011	600, 800	1.82
NBG-18	[20]	600	0.03	1100, 1400	1.85
NBG-18	[59]	750	1	1900, 2200	1.85
NBG-17	[59]	750	1	1500, 1800	1.89
NBG-10	[31]	450	0.00009	25, 50	1.80
NBG-10	[31]	450	0.00009	25, 50	1.80
IG-110	[19]	645	0.099	300, 500	1.77
IG-110	[19]	745	0.9	300, 500	1.77
NBG-25	[19]	645	0.099	500, 600	1.81
NBG-25	[19]	745	0.9	500, 600	1.81
PCEA	[19]	645	0.099	500, 600	1.79
PCEA	[19]	745	0.9	500, 600	1.79
NBG-17	[19]	645	0.099	1500, 1800	1.79
NBG-17	[19]	745	0.9	1500, 1800	1.79
NBG-18	[19]	645	0.099	1900, 2200	1.85
NBG-18	[19]	745	0.9	1900, 2200	1.85
PCEA	ORNL	600	0.03	500, 600	1.79
PCEA	ORNL	600	0.03	500, 600	1.72
PCEA	ORNL	650	0.12	500, 600	1.78
PCEA	ORNL	700	0.4	500, 600	1.79
PCEA	ORNL	700	0.4	500, 600	1.68
PCEA	ORNL	750	1.20	500, 600	1.79
NBG-18	ORNL	600	0.025	1900, 2200	1.85

Grade name	Data reference	Oxid. temp. (°C)	k/r_o (1/s)	Upper and lower β (m^2/m^3)	Bulk density (g/cm^3)
NBG-18	ORNL	650	0.1	1900, 2200	1.85
NBG-18	ORNL	700	0.38	1900, 2200	1.85
NBG-18	ORNL	750	1.2	1900, 2200	1.85
NBG-18	ORNL	655	0.1	1900, 2200	1.84

***Table A2**. Table of specimens and test conditions for oxidation testing.*

Grade name	Sample ID	Set temp (°C)	Meas. temp. (°C)	Diam. (mm)	Height (mm)	Mass (g)	Bulk density, (g/cm^3)
IG-110	2-3	600	597	25.41	25.41	23.26	1.81
IG-110	1-3	650	642	25.39	25.40	23.18	1.80
IG-110	1-4	700	694	25.41	25.32	23.17	1.80
IG-110	2-1	750	753	25.39	25.36	22.96	1.79
IG-110	2-4	600	597	25.44	25.40	23.27	1.80
IG-110	2-5	650	643	25.44	25.39	23.21	1.80
IG-110	3-1	700	693	25.43	25.41	23.12	1.79
IG-110	3-2	750	750	25.41	25.41	23.30	1.81
NBG-18	102	600	595	24.75	24.65	22.93	1.93
NBG-18	101	650	642	25.12	25.02	22.90	1.85
NBG-18	103	700	698	25.01	24.98	22.62	1.84
NBG-18	105	750	752	25.10	24.96	23.00	1.86
NBG-18	106	600	594	25.05	24.95	22.40	1.82
NBG-18	107	650	643	25.10	25.01	22.84	1.85
NBG-18	108	700	698	25.08	25.11	22.93	1.85
NBG-18	109	750	753	25.12	25.04	23.09	1.86
PCEA	2-3	600	595	25.41	25.34	22.98	1.79
PCEA	2-1	650	647	25.41	25.67	22.91	1.76
PCEA	2-5	700	698	25.42	25.50	23.17	1.79
PCEA	2-7	750	752	25.40	25.42	23.04	1.79
PCEA	2-4	600	595	25.42	25.46	23.23	1.80
PCEA	2-2	650	647	25.42	25.51	23.02	1.78
PCEA	2-6	700	698	25.41	25.41	23.07	1.79
PCEA	2-8	750	752	25.41	25.52	23.15	1.79

References

[1] Nightingale, R. E. (2013). *Nuclear Graphite: Prepared under the Auspices of the Division of Technical Information United States Atomic Energy Commission*. Amsterdam: Academic Press.

[2] Burchell, T. D. (1999). *Carbon Materials for Advanced Technologies*. Elsevier.

[3] Windes, W., Burchell, T., and Bratton, R. (2007). *Graphite Technology Development Plan*. INL/EXT-07-13165. Idaho National Laboratory.

[4] Nemeth, N. N., and Bratton, R. L (2010). Overview of statistical models of fracture for nonirradiated nuclear-graphite components. *Nuclear Engineering and Design*, 240, 1, 1–29.

[5] American Society of Mechanical Engineers (2017). American Society of Mechanical Engineers Boiler and Pressure Vessel Code, Section III, Rules for the Construction of Nuclear Facility Components, Division 5, High Temperature Reactors, New York. ASME BPVC.III.5.

[6] Srinivasan, M. (2008). On estimating the fracture probability of nuclear graphite components. *Journal of Nuclear Materials* 381, 1-2, 185–198.

[7] Kelly, B. T. (1981). *Physics of Graphite*. London, Applied Science Publishers.

[8] Kim, E. S., No, H. C., Kim, B. J., and Oh, C. H. (2008). Estimation of graphite density and mechanical strength variation of VHTR during air-ingress accident. *Nuclear Engineering and Design* 238, 4, 837–847.

[9] Contescu, C. I., Mee, R. W., Wang, P., Romanova, A. V., and Burchell T. D. (2014). Oxidation of PCEA nuclear graphite by low water concentrations in helium. *Journal of Nuclear Materials* 453, 1-3, 225–232.

[10] Contescu, C. I., Mee, R. W., Arregui-Mena, J. D., Gallego, N. C., Burchell, T. D., Kane, J. J., and Windes, W. E. (2018). Beyond the classical kinetic model for chronic graphite oxidation by moisture in high temperature gas-cooled reactors. *Carbon* 127, 158–169.

[11] Olasov, L. R., Zeng, F. W., Spicer, J. B., Gallego, N. C., and Contescu, C. I. (2019). Modeling the effects of oxidation-induced porosity on the elastic moduli of nuclear graphites. *Carbon* 141, 304–315.

[12] Matthews, A. C., Kane, J. J., Swank, W. D., and Windes, W. E. (2021). Nuclear graphite strength degradation under varying oxidizing conditions. *Nuclear Engineering and Design* 379, 111245.

[13] Windes, W. E., Burchell, T. D., and Davenport. M. (2020). The advanced reactor technologies (art) graphite R&D program. *Nuclear Engineering and Design* 362, 110586.

[14] Burchell, T., Bratton, R., and Windes, W. (2007). *NGNP Graphite Selection and Acquisition Strategy*. ORNL/TM-2007/153. Oak Ridge National Laboratory.

[15] American Society for Testing and Materials (2019). ASTM D7219-19, Standard Specification for Isotropic and Near-isotropic Nuclear Graphites, ASTM International, West Conshohocken, Pennsylvania.

[16] Arregui-Mena, J. D., Bodel, W., Worth, R. N., Margetts, L., and Mummery, P. M. (2016). Spatial variability in the mechanical properties of Gilsocarbon. *Carbon* 110, 497–517.

[17] Hindley, M. P., Mitchell, M. N., Blaine, D. C., and Groenwold, A. A. (2012). Observations in the statistical analysis of NBG-18 nuclear graphite strength tests. *Journal of Nuclear Materials* 420, 1-3, 110–115.

[18] Contescu, C. I., Guldan, T., Wang, P., and Burchell, T. D. (2012). The effect of microstructure on air oxidation resistance of nuclear graphite. *Carbon* 50, 9, 3,354–3,366.

[19] Smith, R. E., Kane, J. J., and Windes, W. E. (2021). Determining the acute oxidation behavior of several nuclear graphite grades. *Journal of Nuclear Materials* 545, 152648.

[20] Chi, S. H., and Kim, G. C. (2008). Comparison of the oxidation rate and degree of graphitization of selected IG and NBG nuclear graphite grades. *Journal of Nuclear Materials* 381, 1-2, 9–14.

[21] Chi, S. H., and Kim, G. C. (2017). Effects of air flow rate on the oxidation of NBG-18 and NBG-25 nuclear graphite. *Journal of Nuclear Materials* 491, 37–42.

[22] Contescu, C. I., Azad, S., Miller, D., Lance, M. J., Baker, F. S., and Burchell, T. D. (2008). Practical aspects for characterizing air oxidation of graphite. *Journal of Nuclear Materials* 381, 1-2, 15–24.

[23] Lee, J. J., Ghosh, T. K., and Loyalka, S. K. (2017). Comparison of NBG-18, NBG-17, IG-110 and IG-11 oxidation kinetics in air. *Journal of Nuclear Materials* 500, 64–71.

[24] Kane, J. J., Contescu, C. I., Smith, R. E., Strydom, G., and Windes, W. E. (2017). Understanding the reaction of nuclear graphite with molecular oxygen: Kinetics, transport, and structural evolution. *Journal of Nuclear Materials* 493, 343–367.

[25] Contescu, C. I., and Gallego, N. M. *Summary of US DOE R&D Activities on Graphite Oxidation*. ORNL/TM-2021/1892. Oak Ridge National Laboratory.

[26] Kane, J. J., Matthews, A. C., Swank, W. D., and Windes, W. E. (2020). Effects of air oxidation on the evolution of surface area within nuclear graphite and the contribution of macropores. *Carbon* 166, 291–306.

[27] Wang, P., Contescu, C. I., Yu, S. and Burchell, T. D. (2012). Pore structure development in oxidized IG-110 nuclear graphite. *Journal of Nuclear Materials* 430, 1-3, 229–238.

[28] Kane, J. J., Karthik, C., Ubic, R., Windes, W. E., and Butt, D. P. (2013). An oxygen transfer model for high purity graphite oxidation. *Carbon* 59, 49–64.

[29] Contescu, C. I., Strizak, J. P., Guldan, T. R., and Burchell, T. D. (2010). *Effect of Air Oxidation on Pore Structure Development and Mechanical Properties of Nuclear Graphite*. ORNL/TM-2010/197. Oak Ridge National Laboratory.

[30] Huang, W.-H., Tsai, S.-C., Yang, C.-W., Kai, J.-J. (2014). The relationship between microstructure and oxidation effects of selected IG-and NBG-grade nuclear graphites. *Journal of Nuclear Materials* 454, 149–158.

[31] Hinssen, H.-K., Kühn, K., Moormann, R., Schlögl, B., Fechter, M., and Mitchell, M. (2008). Oxidation experiments and theoretical examinations on graphite materials relevant for the PBMR. *Nuclear Engineering and Design* 238, 11, 3,018–3,025.

[32] Kane, J. J., Matthews, A. C., Orme, C. J., Contescu, C. I., Swank, W. D., and Windes, W. E. (2018). Effective gaseous diffusion coefficients of select ultra-fine, super-fine and medium grain nuclear graphite. *Carbon* 136, 369–379.

[33] Lo, I-H., Tzelepi, A., Patterson, E. A., and Yeh, T.-K. (2018). A study of the relationship between microstructure and oxidation effects in nuclear graphite at very high temperatures. *Journal of Nuclear Materials* 501, 361–370.

[34] Paul, R. M. (2021). Application of a three-dimensional random pore model for thermal oxidation of synthetic graphite. *Journal of Nuclear Materials* 543, 152589.

[35] Paul, R. M., and Morral, J. E. (2018). A 3D-Random pore model for the oxidation of graphite with closed porosity. *Journal of Nuclear Materials* 509, 425–434.

[36] Paul, R. M., and Morral, J. E. (2018). A 3D random pore model for the oxidation of graphite with open porosity. *Journal of Nuclear Materials* 499, 344–352.

[37] American Society for Testing and Materials (2015). ASTM D7542-15, Standard Test Method for Air Oxidation of Carbon and Graphite in the Kinetic Regime, ASTM International, West Conshohocken, Pennsylvania.

[38] Bhatia, S. K., and Perlmutter, D. D. (1980). A random pore model for fluid-solid reactions: I. Isothermal, kinetic control. *AIChE Journal* 26, 3, 379–386.

[39] Gavals, G. R. (1980). A random capillary model with application to char gasification at chemically controlled rates. *AIChE Journal* 26, 4, 577–585.

[40] Avrami, M. (1939). Kinetics of Phase Change. I General Theory, *Journal of Chemical Physics* 7, 1103.

[41] Kolmogorov, A. N. (1937). On the Statistical Theory of the Crystallization of Metals, Bull. Acad. Sci. USSR. Math. Ser1, 355–359.

[42] Johnson, W. A., and Mehl, R. F. (1939). Reaction Kinetics in Processes of Nucleation and Growth. *Trans. AIME* 135, 396–415.

[43] Wichner, R. P., and Ball, S. J. (1999). *Potential Damage to GasCooled Graphite reactors Due to Severe Accidents.* ORNL/TM-13661. Oak Ridge National Laboratory.

[44] Fuller, E. L., and Okoh, J. M. (1997). Kinetics and mechanisms of the reaction of air with nuclear grade graphites: IG-110. *Journal of Nuclear Materials* 240, 3, 241–250.

[45] El-Genk, M. S., and Tournier, J-M. P. (2012). Comparison of oxidation model predictions with gasification data of IG-110, IG-430 and NBG-25 nuclear graphite. *Journal of Nuclear Materials* 420, 1-3, 141–158.

[46] Bhatia, S. K., and Perlmutter, D. D. (1981). A random pore model for fluid-solid reactions: II. Diffusion and transport effects. *AIChE Journal* 27, 2, 247–254.

[47] Bhatia, S. K., and Vartak, B. J. (1996). Reaction of microporous solids: The discrete random pore model. *Carbon* 34, 11, 1,383–1,391.

[48] Gupta, J. S., and Bhatia, S. K. (2000). A modified discrete random pore model allowing for different initial surface reactivity. *Carbon* 38, 1, 47–58.

[49] Delikouras, E. A., and Perlmutter, D. D. (1991). Inaccessible porosity in gasification reactions under kinetic control. *AIChE Journal* 37, 11, 1,607–1,612.

[50] Smith, I. W. (1978) The intrinsic reactivity of carbons to oxygen. *Fuel* 57, 7, 409–414.

[51] Zheng, G., Xu, P., Sridharan, K., and Allen, T. (2014). Characterization of structural defects in nuclear graphite IG-110 and NBG-18. *Journal of Nuclear Materials* 446, 1, 193–199.

[52] Gallego, N. C., Arregui-Mena, J. D., and Contescu, C. I. (2021). Probing basal planes and edge sites in polygranular nuclear graphite by gas adsorption: Estimation of active surface area. *Carbon* 179, 633–645.

[53] Gallego, N., Contescu, C. I., and Keiser, J. (2020). *Progress Report on Graphite-Salt Intrusion Studies*. ORNL/TM-2020/1621. Oak Ridge National Laboratory.

[54] Wade-Zhu, J., Krishna, R., Bodey, A. J., Davies, M., Bourne, N. K., Rau, C., Davies, B., et al. (2020). 4D synchrotron X-ray microtomography of fracture in nuclear graphite after neutron irradiation and radiolytic oxidation. *Carbon* 168, 230–244.

[55] Kim, E. S., Lee, K. W., and No, H. C. (2006). Analysis of geometrical effects on graphite oxidation through measurement of internal surface area. *Journal of Nuclear Materials* 348, 1-2, 174–180.

[56] Fujita, I., Eto, M., Ohsaki, H., Shibata, T., Konishi, T., Yamaji, M., Kunimoto, E., and Sumita, J. (2013). *Evaluation of oxidation characteristics of fine-grained graphites (IG-110 and IG-430) for very high temperature reactor. Changes in density distribution and compressive strength caused by air-oxidation*. JAEA-RESEARCH--2013-004. Japan Atomic Energy Agency.

[57] Cho, K-Y., Kim, K-J., Lim, Y-S., Chung, Y-J., and Chi, S-H. (2006). Specimen geometry effects on oxidation behavior of nuclear graphite. *Carbon Letters* 7, 3, 196–200.

[58] Oh, C. H., Kim, E. S., No, H. C., and Cho. N. Z. *Experimental Validation of Stratified Flow Phenomena, Graphite Oxidation, and Mitigation Strategies of Air Ingress Accidents*. INL/EXT-08-14840. Idaho National Laboratory.

[59] Smith, R. E., *Comparison of Oxidation Performance of Graphite Samples in TGA versus Vertical Furnace*. INL/EXT-19-54584, Idaho National Laboratory.